Influence of Blend Composition on Phase Separation and Dewetting of Thin Polymer Blend Films

P. Müller-Buschbaum,*,† J. S. Gutmann,‡ and M. Stamm‡,§

TU München, Physik-Department LS E13, James-Franck-Str.1, 85747 Garching, Germany, and Max-Planck-Institut für Polymerforschung, Ackermannweg 10, 55128 Mainz, Germany

Received July 6, 1999; Revised Manuscript Received March 28, 2000

ABSTRACT: Thin polymer blend films of deuterated polystyrene (dPS) and poly(*p*-methylstyrene) (PpMS) with several blend compositions between 95:5 and 5:95 were prepared on top of glass substrates. The samples were examined right after preparation and after annealing. Their surface morphology was investigated with scanning force microscopy (SFM). A statistical analysis of the SFM data yielded the rms roughness as well as the most prominent in-plane length parallel to the sample surface. Information about the density profile perpendicular to the sample surface is gained from neutron reflectivity measurements in the region of total external reflection. Right after preparation dPS segregates to the air interface, while during annealing at a temperature above the glass transition temperature of both polymers, PpMS builds up a top layer toward the interfaces. Depending on blend composition and annealing time, different surface topographies are evolving. The examined film thicknesses are below a critical thickness, ensuring that composition fluctuations directed normal to the surface are suppressed. However, the small film thickness constrains kinetics largely to two dimensions. The surface morphology is controlled by an interplay between phase separation and dewetting.

Introduction

Thin polymer films are widely used in electronics, optics, and biotechnology. The broad range of applications requests polymer films with very different surface morphologies. This includes smooth and uniform surfaces, a dedicated enhanced surface roughness, or special surface patterns with varying in-plane lengths. With homopolymer films this broad application range usually requires a special surface treatment or even the synthesis of a new polymer for every particular application. An economical alternative can be the preparation of particular morphologies by the blending of two homopolymers. The behavior of polymer blend films is qualitatively different from that of binary mixtures in the bulk.[1] Because of the existence of two boundary interfaces and generally a preferential segregation of one or the other component of the blend to the interfaces, a development of composition waves normal to the surface can be induced. This surface directed spinodal decomposition can propagate some wavelengths into the film before decaying into an isotropic bicontinuous spinodal bulk pattern. In thin blend films with film thicknesses below a critical thickness these composition waves normal to the surface are suppressed.[2−5] The blend phase separation within the film is accompanied by undulations of the contour of the free boundary, as observed in the case of symmetrical surface segregation.[6] We investigate thin polymer blend films of deuterated polystyrene (dPS) and poly(*p*-methylstyrene) (PpMS) in a thickness regime where surface-directed spinodal decomposition is suppressed. Additionally, the films are sufficiently thick that confinement effects are negligible. Both components dPS and PpMS differ only by one methyl group, which results in a small interaction parameter.[7,8] As a result of this small incompatibility, the accessible regime of possible surface morphologies is enlarged. Smooth and structureless surfaces can be prepared in this case, while in strongly incompatible blend films right after preparation the morphology is dominated by a well-pronounced surface pattern. In the weakly incompatible system dPS/PpMS the surface morphology is controlled by an interplay between phase separation and dewetting.[9] Depending on the blend composition and the annealing time, different surface topographies are generated. The surface morphologies are examined with scanning force microscopy (SFM) and statistically analyzed in terms of rms roughness and most prominent in-plane length scale. Information about the composition profile perpendicular to the sample surface is gained from neutron reflectivity measurements. This supplements the information about the chemical composition of the free surface, gained from previous static SIMS measurements.[9]

The paper is structured as follows: The introduction is followed by an Experimental Section describing the sample preparation and the techniques used. The next section deals with the interpretation of the neutron scattering measurements. Then the SFM measurements are reported. A discussion and summary conclude the paper.

Experimental Section

Sample Preparation. As substrates we used float glass plates which were cleaned prior to the spin-coating. The cleaning bath consists of 100 mL of 80% H_2SO_4, 35 mL of H_2O_2, and 15 mL of deionized water (for 15 min at 80° C). Afterward, the substrates were rinsed in deionized water several times and dried with compressed nitrogen. Immediately before coating the dry substrates were flushed with fresh

† TU München.
‡ Max-Planck-Institut für Polymerforschung.
§ Present address: IPF Dresden e.V., Hohe Str. 6, 01069 Dresden, Germany.
* To whom correspondence should be addressed. Fax (49)89-289-12473; e-mail muellerb@physik.tu-muenchen.de.

10.1021/ma991073+ CCC: $19.00
Published on Web 06/07/2000

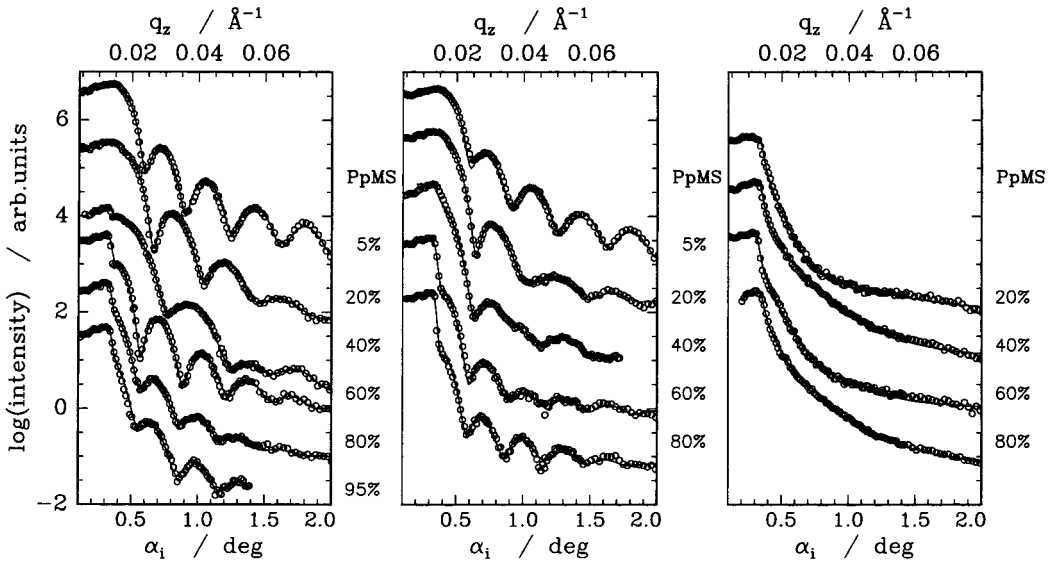

Figure 1. Specular neutron reflectivities (circles) and fits (solid lines) versus angle of incidence α_i of thin PpMS:dPS blend films on float glass substrates right after preparation (left side), after 8 h of annealing at $T = 161°$ C (center), and after 261 h of annealing at $T = 161°$ C (right side). The blend composition is varied from top to bottom. The amount of PpMS is varied between 5% and 95% as labeled in the graph. For clarity, the curves are shifted by 1 order of magnitude against each other. The sample with PpMS:dPS = 95:5 was not measured after annealing due to the shortage of neutron beam time.

toluene, and then the thin films were prepared by spin-coating (1950 rpm for 30 s) a toluene solution of the polymer blend onto the glass substrate. Deuterated polystyrene (dPS) with a molecular weight $M_w = 157\,000$ g/mol and a narrow molecular weight distribution $M_w/M_n = 1.09$ as well as poly(*p*-methylstyrene) (PpMS) with a molecular weight $M_w = 157\,000$ g/mol and $M_w/M_n = 1.06$ are used. Several blend compositions (PpMS:dPS = 95:5, 80:20, 60:40, 40:60, 20:80, and 5:95 by weight) with a fixed film thickness were prepared. From X-ray reflectivity measurements right after preparation the film thickness of the presented blend films was determined to be $l = 460 \pm 25$ Å. Slight thickness variations are due to changes in the blend composition. All prepared samples have a thickness above 4 times the radius of gyration of the unperturbed molecule, $l_{tot} > 4R_g$, which ensures that confinement effects are negligible. The samples were examined as prepared and then annealed under vacuum for 8 and 261 h at 161° C. The intermediate annealing step of 8 h was chosen well within the time range during which the surface morphology is dominated by phase separation.[9] After the large annealing step of 261 h it is influenced by an additional dewetting process.[9] The annealing temperature corresponds to a temperature well within the two-phase regime of the dPS/PpMS phase diagram. To check the reproducibility of observed structures, six samples of each composition were prepared and examined. The as-cast samples as well as the annealed samples exhibit reproducible morphologies as described below.

Neutron Reflectivity. The neutron reflectivity experiments in the region of total external reflection were performed at the EVA beamline at the ILL (Grenoble) with a chosen wavelength of $\lambda = 5.5$ Å. With a graphite monochromator PG(002) and a slit collimating system, a beam divergence of 0.018° and a wavelength resolution of $\Delta\lambda/\lambda = 0.012$ were chosen. A sample−detector distance of 1920 mm was installed. We used a one-dimensional linear wire detector. Thus, the nonspecular as well as the specular intensity was recorded. A further description of the reflectometer setup is given in ref 10. Using a matrix formalism, model fits to the data were calculated.[11] The interfaces of homogeneous layers are described by a tanh refractive index profile with the interfacial roughness σ. This profile is commonly used for substrates[12] as well as for the interface between polymers.[13] The interface profile of the dewetted layer differs from the one of a homogeneous layer. It was parametrized in accordance with the results of the analysis of the scanning force microscopy and not varied in the fit. Because reflectivity measurements probe the density profile laterally averaged over the coherently illuminated sample, holes in the film cause a reduction of the apparent scattering density of the material.

Scanning Force Microscopy. Micrographs of the blend films were recorded with a PARK Autoprobe CP atomic force microscope (AFM). We used silicon gold-coated conical cantilevers, with a spring constant of ≅1.6 N m^{-1}. To minimize tip-induced sample degradation all measurements were performed in noncontact mode. The image acquisition was done in air at room temperature. Several images were measured for each sample. The scan range was chosen between 5 μm × 5 μm to achieve a high resolution and 100 μm × 100 μm to detect possible superstructures. The background due to the scanner tube movement is fully subtracted from the data to determine the values of the rms roughness over the complete scan area. The rms roughness values were calculated for each individual scan range. After a Fourier transformation from the surface data of each sample and scan range the two-dimensional power spectral density function (PSD) is calculated and radially averaged. Combining the data of different scan sizes yields a master curve and thus enlarges the range of accessible inverse length scales compared to one individual PSD. The resulting master curve as a function of inverse length scales is equivalent to a scattering signal and thus pictures the existence of any most prominent in-plane length scale within the resolvable range. With the rms roughness and the master curve the sample surface is described in a statistical sense.

Results

Neutron Reflectivity. Before annealing and after both annealing steps the polymer blend samples were examined using neutron reflectivity. The data together with a fit using the model explained in the Experimental Section are displayed in Figure 1. From the left to the right the data of the as-prepared, 8 h annealed and 261 h annealed samples are presented. From the bottom to the top the content of PpMS decreases from 95% to 5%. The shift of the critical angle toward larger incident angles α_i pictures the respective increase of deuterated dPS, which has the larger scattering length density as compared to that of PpMS (δ(dPS)/δ(PpMS) = 4.2). Compared to the as-prepared samples, the fringes in the reflectivity curves after 8 h annealing are damped out

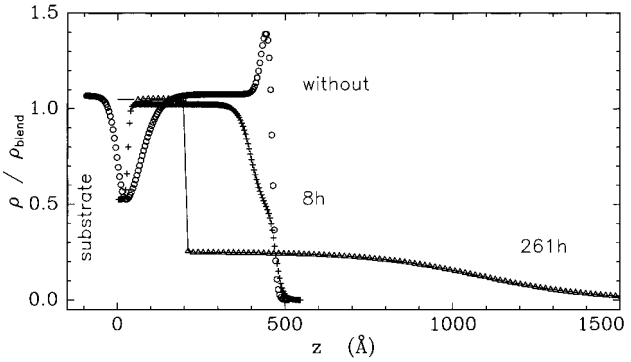

Figure 2. Examples of three different density profiles of the PpMS:dPS = 60:40 blend thin film. The glass substrate surface is located at $z = 0$. The density is normalized to the mean value of the bulk blend dPS−PpMS. The density profiles of the sample right after preparation (circles) and the one after 8 h of annealing (crosses) exhibit two enrichment layers. Note that due to the big roughness values of the polymer−polymer interface as well as of the polymer−air interface, the density of the PpMS layer seems to be increased and the density of the dPS layer correspondingly decreased. The density profile of the dewetted sample after 261 h annealing time (triangles) pictures the big roughness due to large drops.

slightly, which is due to increasing surface roughness. A further increasing surface roughness (after the second annealing step) basically smears out possible fringes in the reflectivity curve. Comparing for example the reflected intensities of the PpMS:dPS = 40:60 sample pictures, the drastic changes inside the sample during the first 8 h of annealing. The fit (solid line) to the data provides a density profile which pictures the internal structure perpendicular to the sample surface and provides an additional information to the surface topography as observed with the SFM.

Figure 2 displays three typical density profiles obtained at one fixed blend composition: one of the homogeneous blend films (without), one of the films well within the phase separation region (8 h), and one of the dewetted samples (261 h). The density values are normalized to the mean blend density (in the presented example PpMS:dPS = 60:40). The density profile of the sample right after preparation shows an enrichment of PpMS at the substrate surface and an enrichment of dPS at the air interface. The thickness of the PpMS enrichment layer (65 ± 5 Å) is nearly twice the thickness of the dPS enrichment layer (33 ± 4 Å). Therefore, the intermediate mixed blend film has a slightly increased density compared to the theoretical value calculated from the blending ratio, and the part of the density profile in Figure 2 shows values slightly above $\rho/\rho_{blend} = 1$. Because of the smearing of the interface roughness, the values of pure dPS ($\rho/\rho_{blend} = 1.8$) and pure PpMS ($\rho/\rho_{blend} = 0.4$) are not reached.

After 8 h of annealing at $T = 161°$ C the sample state is well within the phase separation process. As it can be seen from the density profile in Figure 2, the PpMS enrichment layer near the substrate has shrunken (thickness 32 ± 3 Å) and the dPS enrichment at the surface is replaced by a PpMS enrichment. Thus, PpMS has segregated at both interfaces. Nearly the whole film exhibits the mean blend bulk density. A small increase in surface roughness as compared to the samples right after preparation is detected.

The big surface roughness of the dewetted film (261 h) cannot be measured with neutron scattering. Therefore, the surface near part of the density profile has to be modeled from the bearing analysis of the SFM measurements under the boundary condition of mass conservation:[14] The height profile resulting from SFM data is transferred into a scattering length density profile. During the fit of the neutron data the shape of this profile is kept fixed. This yields a strongly smeared out density profile due to the drop structure. Whether the drops consist of dPS or PpMS cannot be extracted from this method. In addition, it has to be noted that the calculated density profile of the 261 h annealed samples does not have the same accuracy as the ones of the as prepared or 8 h annealed samples. The presence of a homogeneous layer below the drop structure was confirmed previously with X-ray scattering.[9] Due to the missing sensitivity of the fit to featureless reflectivity data, we cannot extract the internal structure of this layer. Because its thickness exceeds the value which would be possible due the total content on dPS, we can conclude that it has to contain PpMS as well.

Irrespective of the blend composition, a quite similar behavior was observed for all other investigated samples. The individual drop size depends on the blend composition of the sample. Consequently, we do not observe a dewetting of the complete film from the glass substrate. Of course, the thicknesses of the enrichment layers change with variation of the blend composition.

Scanning Force Microscopy. With SFM the topography of the sample surface is measured with high resolution. Figures 3−5 display pictures of the examined blend compositions after each annealing step. The shown scan range of 5 μm × 5 μm is needed due to the small evolving surface structures. Right after preparation (Figure 3) all six compositions examined have the smallest surface roughness. Whereas the samples, with a composition closest to homopolymers, exhibit smooth and featureless surfaces (Figure 3a,f), the other blend sample morphologies are dominated by small droplets (Figure 3b) and small (Figure 3e) or large (Figure 3d) holes of a spinodal-like surface pattern (Figure 3c). This very regular surface topography built up during the spin-coating and was previously similarly observed in the case of other polymer blend systems.[15−17] Near the symmetric blend composition the largest surface structures evolve.

After the first annealing step (Figure 4) the rms surface roughness of the blend samples increased slightly. This can be assumed to arise from the progress of the phase separation process. While the surface morphology of the sample with PpMS:dPS = 60:40 (Figure 4c) and PpMS:dPS = 40:60 (Figure 4d) remains unchanged despite a deepening, it is changed in the other samples. The small holes have grown to larger, merging ones (Figure 4e), and the droplets have merged to larger ones (Figure 4b). The observed structures are less regular, and the peak-to-valley distances are increased.

After the second annealing step (Figure 5) five samples were dewetted. Thus, the evolved structures are much larger. Figure 5 shows the same scan range as Figures 3 and 4 to enable a better comparison. Three samples show large drops with micrometer diameter (Figure 5c−e). From the width and height of the measured drops the presence of an additional underlying layer can be concluded indirectly. If a dewetting of the complete film would have been present, one would

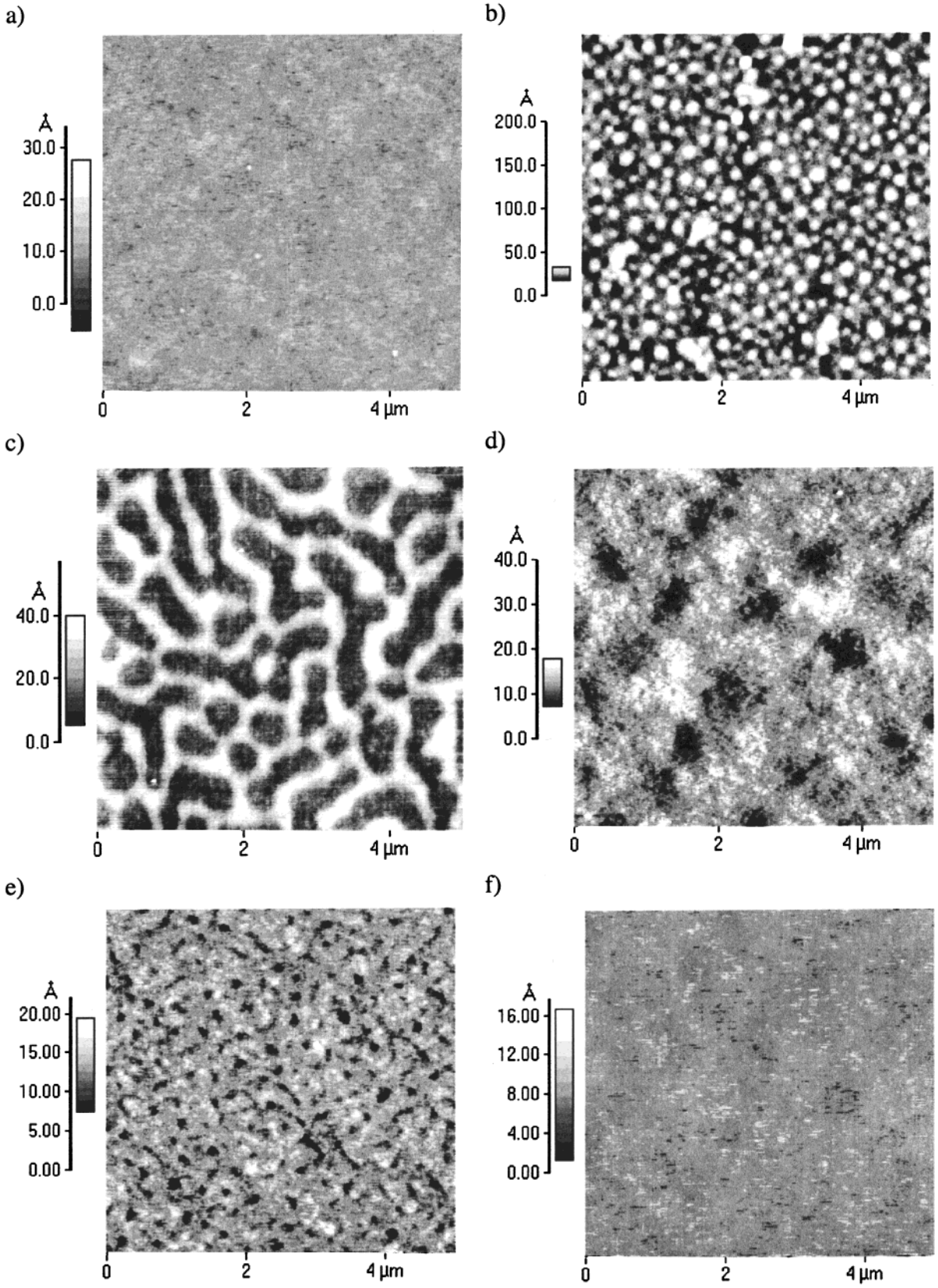

Figure 3. SFM images of the PpMS:dPS blend thin film at six different blend compositions right after preparation: PpMS:dPS = 95:5 (a), 80:20 (b), 60:40 (c), 40:60 (d), 20:80 (e), and 5:95 (f). The scan range of each picture is 5 μm × 5 μm whereas the *z*-scale is different for each pattern ((a) 33 Å, (b) 18 Å, (c) 36 Å, (d) 11 Å, (e) 11 Å, and (f) 13 Å) to show the in-plane structure more clearly.

have observed drops with 3.5 μm diameter and heights larger than 5000 Å due to volume conservation. Remarkably on top of the samples close to homopolymer composition (Figure 5a,f) small droplets have formed. They result from a dewetted ultrathin polymer layer. Previously nano-dewetting structures of homopolymers have been observed on top of solid surfaces.[18,19] The volume ratio calculated from the droplet parameters

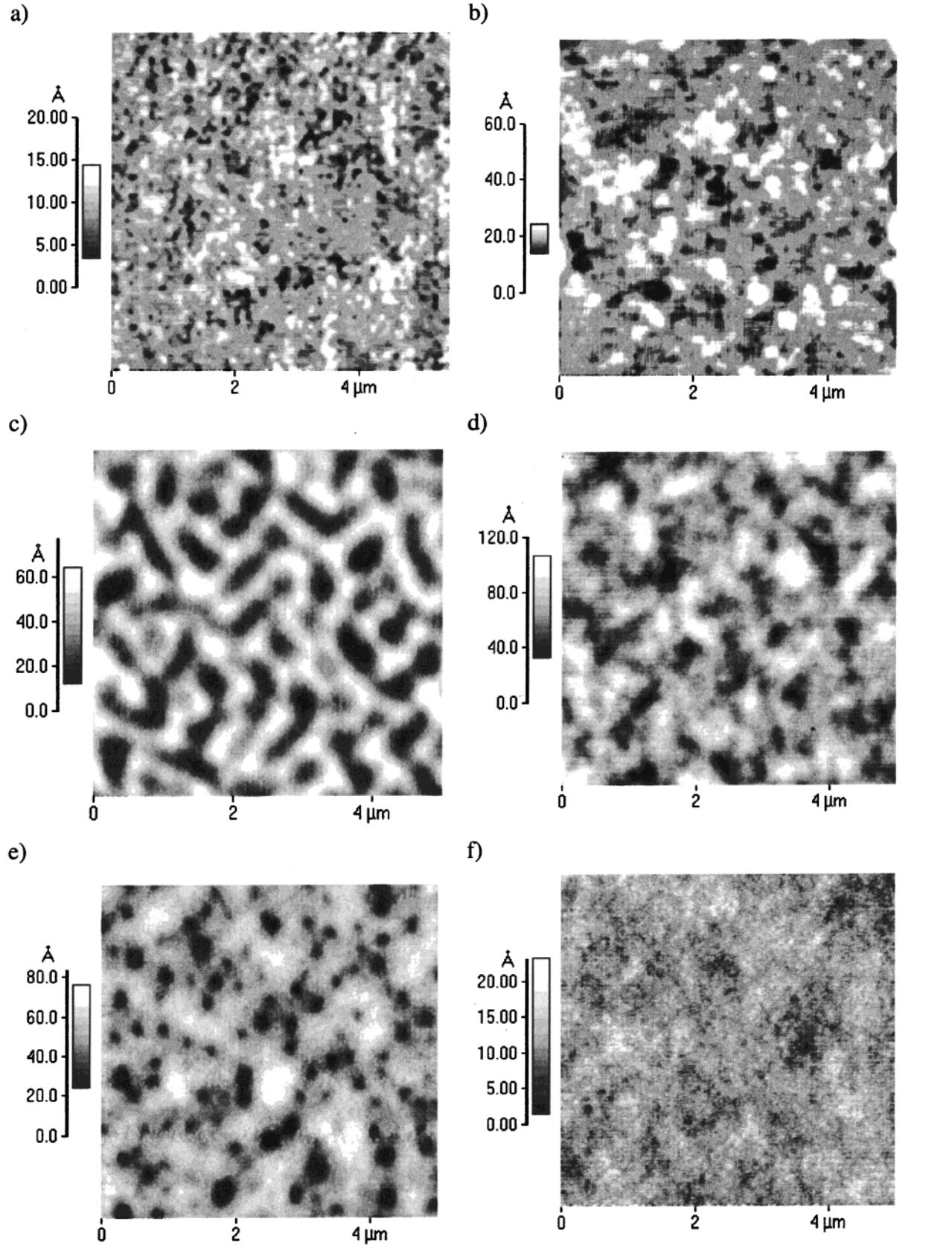

Figure 4. SFM images of the PpMS:dPS blend thin film at six different blend compositions after 8 h of annealing: PpMS:dPS = 95:5 (a), 80:20 (b), 60:40 (c), 40:60 (d), 20:80 (e), and 5:95 (f). The scan range of each picture is 5 μm × 5 μm whereas the *z*-scale is different for each pattern ((a) 11 Å, (b) 11 Å, (c) 53 Å, (d) 76 Å, (e) 53 Å, and (f) 22 Å) to show the in-plane structure more clearly.

(Figure 5a: height $h = 511$ Å, radius $r = 2350$ Å; Figure 5f: height $h = 90$ Å, radius $r = 1570$ Å) exceeds the amount of the corresponding minor component, which suggests that these droplets do not consist exclusively of one pure component, PpMS or dPS. Therefore, all observed dewetting structures behave similarly despite

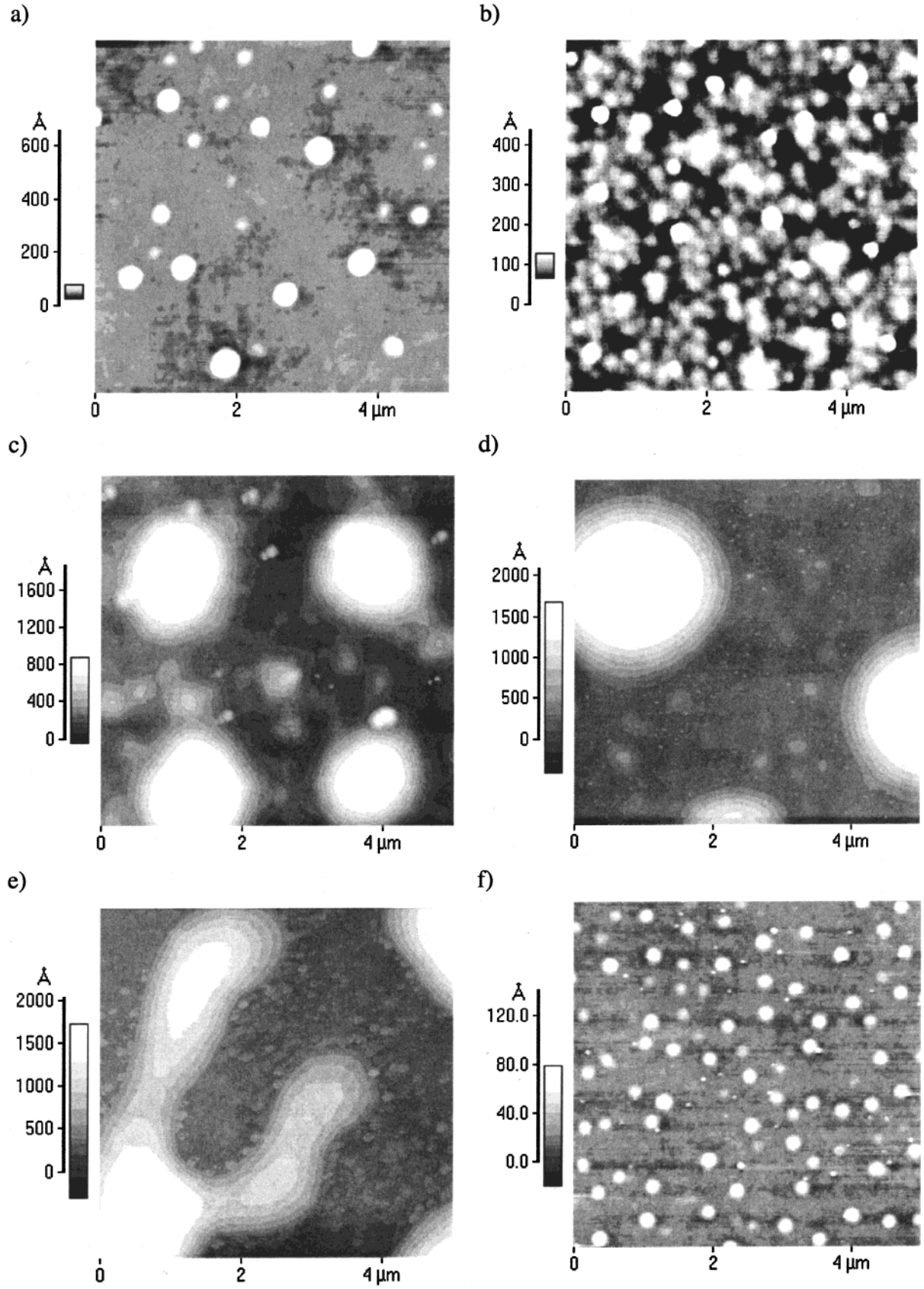

Figure 5. SFM images of the PpMS:dPS blend thin film at six different blend compositions after 261 h of annealing: PpMS:dPS = 95:5 (a), 80:20 (b), 60:40 (c), 40:60 (d), 20:80 (e), and 5:95 (f). The scan range of each picture is 5 μm × 5 μm whereas the *z*-scale is different for each pattern ((a) 62 Å, (b) 69 Å, (c) 946 Å, (d) 2113 Å, (e) 2060 Å, and (f) 100 Å) to show the in-plane structure more clearly.

their actual size. The irregular shape, observed for the sample with PpMS:dPS = 20:80 (Figure 5e), suggests that the dewetting process is not completed. In Figure 5b still a rough surface is present. In Table 1 the characteristics of the evolving surface morphologies are listed.

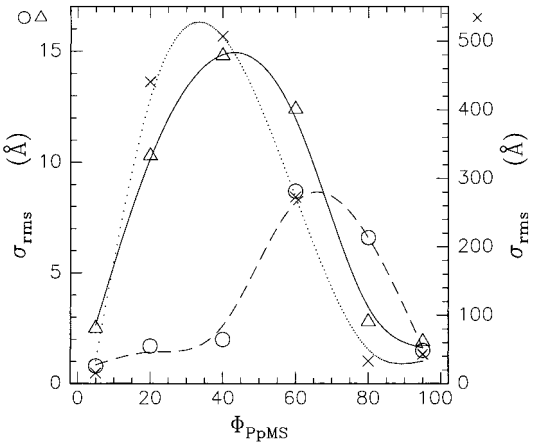

Figure 6. Resulting surface rms roughness from the SFM measurements right after preparation (circles), after 8 h annealing (triangles), and after 261 h annealing (crosses) as a function of the PpMS blend composition Φ_{PpMS}. The lines are guides to the eye to underline the shift in the maximum roughness toward smaller values of Φ_{PpMS} due to annealing.

Table 1. Surface Morphology As Observed with the SFM for the Examined Blend Compositions Right after Preparation (without), after 8 h Annealing and after 261 h Annealing at $T = 161$ °C

PpMS:dPS	without	8 h	261 h
95:5	smooth	rough	droplets
80:20	droplets	holes	irregular
60:40	continuous	continuous	drops
40:60	holes	holes	drops
20:80	dimples	holes	drops
5:95	smooth	rough	droplets

Discussion

The polymer−polymer interaction parameter of dPS and PpMS $\chi = A + B/T$ with $A = -0.011 \pm 0.002$ and $B = 6.8 \pm 1$ K[8] yields $N\chi \cong 6.6$, which displays the weak incompatibility of the investigated system. The small film thickness additionally makes the system more mixable as compared to the bulk.[20] Thus, right after preparation only small surface structures evolve.[21]

With neutron reflectivity the density profile perpendicular to the sample surface[11,22−24] and thus the internal film structure is determined. In the case of a large surface roughness the information about the shape of the density profile is gained from the SFM measurements. Neutron reflectivity averages laterally, and the in-plane surface morphology of the samples is investigated with SFM. Neglecting the actual shape of the surface structure the rms roughness σ_{rms} is an adequate measure for a surface description in a statistical sense. The values obtained from the SFM measurements are plotted in Figure 6 versus the blend content of PpMS Φ_{PpMS}. Because the rms roughness values are drastically enlarged due to the additional dewetting process during the second annealing step, all data are plotted in one graph with two different *y*-axis scalings. The data points of the as-prepared samples (circles) and of the 8 h annealed samples (triangles) belong to the left *y*-axis, whereas the one of the 261 h annealed ones (crosses) belong to the right *y*-axis in Figure 6. The analysis of SFM pictures with enlarged scan ranges up to 100 μm yields the same rms roughness values as plotted in Figure 6. The lines are guides to the eye, to picture the shift of the maximum roughness toward smaller PpMS content after annealing. While the rms roughness represents a statistical measure perpendicular to the sample surface, statistical information about the structure parallel to the sample surface is equally desirable. For this reason we turn to a closer inspection of the power spectral density computed from the SFM images. Rotationally isotropic distributed surface morphologies give rise to circular-shaped two-dimensional power spectral density functions (PSD) after Fourier transformation. Surface structures created during the early stages of the spin-coating process, which is dominated by shear flow, exhibit a different morphology: Structures are starlike arranged with a center equal to the center of the rotation.[21] Consequently, the PSD has no radial symmetry and an elliptic shape. In the case of a circular shape a radially averaging of the two-dimensional PSD results in a one-dimensional PSD with enhanced statistics. Combining these one-dimensional PSDs of different scan ranges yields a master curve as a function of inverse lengths *s*. For each individual sample, composition, and annealing time such a master curve was calculated. From these master curves a possible preferential in-plane length scale is detectable.[21,25] If the master curve exhibits a peak in the resolvable range, it is originating from a dominant in-plane length $\Lambda_{PSD} = 1/s$. Beside the rms roughness this length is a second characteristic of the surface morphology. Figure 7 shows the master curve as a function of *s* for one typical example where the morphology is dominated by one prominent in-plane length. The peak position is marked with an arrow, and the inset shows the two-dimension power−spectral density data as a gray scale contour plot (dark areas mark high intensity). If no peak is observable in the master curve, we take $\Lambda_{PSD} = 0$. In Figure 8 all determined length scales Λ_{PSD} are plotted as a function of the blend composition. As in Figure 6, the data from the as-prepared samples are plotted with circles, the data after 8 h of annealing with triangles, and the data after 261 h of annealing with crosses, and the lines are guides to the eye.

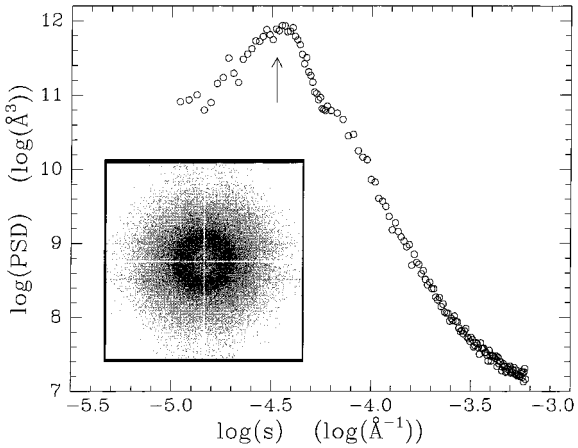

Figure 7. Radially averaged two-dimensional power spectral density functions (PSD) combined to a master curve as a function of inverse in-plane lengths *s*. The marked peak (arrow) results from a dominant in-plane length. The inset shows a contour gray scale plot of the two-dimensional power spectral density function. Dark areas represent high intensities.

As can be seen from Figures 6 and 8, the structures right after preparation are apparently not the equilibrium ones as observed in the blend system PS:PBrS.[26,27] The surface structures are dominantly due to dPS which explains the shift of σ_{rms} and Λ_{PSD} toward smaller PpMS content during annealing.

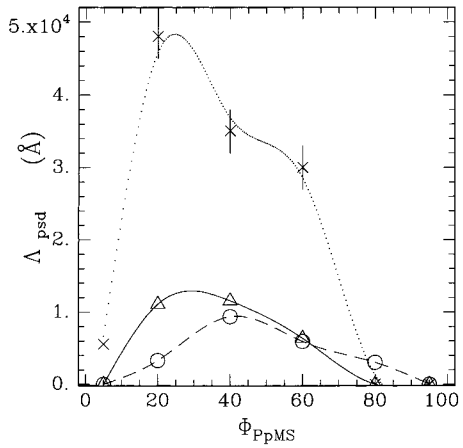

Figure 8. Dominant in-plane length Λ_{PSD} determined from the position of the peak of the master curve resulting from the SFM measurements. The data right after preparation (circles), after 8 h annealing (triangles), and after 261 h annealing (crosses) are shown as a function of the PpMS blend composition Φ_{PpMS}. The lines are guides to the eye. Only for large values of Λ_{PSD} do the error bars exceed the symbol size as shown by the vertical lines.

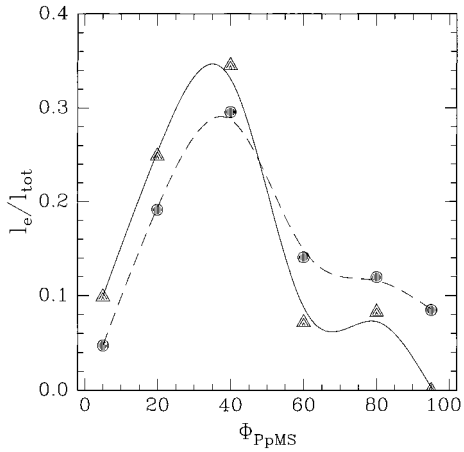

Figure 9. Thickness of the enrichment layers l_e normalized to the total film thickness l_{tot} as a function of the PpMS blend composition Φ_{PpMS}. The enrichment layer near the substrate (circles) contains PpMS, and the one at the surface (triangles) contains dPS right after preparation. The lines are guides to the eye.

As-Prepared Samples. Spin-coating is a dynamic process which created nonequilibrium structures as the solvent evaporates. The rate of solvent evaporation plays a crucial role in the installing topography[15] as well in the internal film structure. It influences the viscosity of the highly concentrated polymer solution and thus the competition between diffusive and hydrodynamic growth. The observed continuous structure (Figure 3c) indicates pure diffusive growth in combination with a large viscosity (compare lattice Boltzmann simulations in ref 28). The formation of continuous layers indicates a segregation process that proceeds into the direction of the surface. The thickness of the enrichment layers l_e normalized to the total film thickness l_{tot} is plotted versus the blend content of PpMS, Φ_{PpMS}, in Figure 9. The enrichment layer near the substrate (circles) contains PpMS and the one at the surface (triangles) contains dPS as discussed above. Interface enrichment right after preparation was not observed in previous experiments.[9] This may be attributed to changes in the preparation conditions (slower spinning speed) or differences in the interaction between the substrate (Si or glass) and the polymer blend solution. In addition, the detection of a thin surface segregation layer of dPS might have been difficult with X-ray scattering[9] due to the weak contrast between the two polymer components. Segregation of dPS to the air interface is a nonequilibrium phenomena, because of the higher surface tension of dPS, $\gamma_{dPS} = 40$ mN m^{-2}, compared to that of PpMS, $\gamma_{PpMS} = 35$ mN m^{-2} (values refer to room temperature[29]). The thickness of the dPS layer is small compared to the total amount of dPS available in the blend. An additional monomolecular top layer of PpMS on top of this dPS enrichment layer, as detected with static SIMS,[9] cannot be excluded due to the limited spatial resolution of the neutron scattering experiment. Enrichment of PpMS near the glass substrate is energetically favored. Previously, a homogeneous PpMS layer near the substrate was observed on top of silicon substrates after annealing.[9] In the samples with the low PpMS content nearly all of the PpMS segregates to the substrate right after preparation. Thus, lowering the spinning speed during the spin-coating allows the phase separation to proceed at the solution−substrate interface for a longer time. A similar behavior was observed in the blend system dPS:PBrS.[15] Additionally, the solvent evaporation at the solution−air interface destabilizes the upper part of the film and creates the marked surface morphologies (see Figure 3). Holes formed in the upper part of the film are filled by the lower liquid phase (Figure 3e). As the holes grow (Figure 3d), a coalescence into a regular and continuous surface structure (Figure 3c) is possible. Increasing the amount of PpMS this continuous structure becomes unstable and decays into droplets (Figure 3b). Despite the smooth surfaces (Figure 3a,d) all surface morphologies exhibit a ring in a Fourier pattern analysis, which shows that one preferential length scale is always present. This suggests an in-plane domain formation primarily driven by a spinodal process. The domain growth is constrained to a quasi-two-dimensional configuration due to the thickness of the film: Domains start to grow in three dimensions until their size reaches the thickness of the layer, which itself decreases as a function of time during solvent evaporation.[30] The observed variation of domain size with film thickness will be reported elsewhere.[31]

After 8 h Annealing. Surface structures formed after spin-coating are not in thermodynamical equilibrium. Figure 6 pictures the increase of rms roughness and the shift of the maximum of the roughness distribution toward reduced PpMS content Φ_{PpMS} after annealing. As determined from the neutron reflectivity, PpMS segregates to both interfaces, which leads to a reduction of the enrichment layer thickness, of the one near the substrate, forced by mass conservation. The segregation of PpMS at the surface during early annealing stages was reported previously[9] for a symmetric blend composition PpMS:dPS = 50:50. The thermodynamically favored state is composed mainly of the component with the lower surface energy, PpMS, segregated to the surface, and the corresponding enrichment layer has to build up. Consequently, the polymer has to be transported through the film. In films made of a blend with lower PpMS content more material has to migrate over larger distances. Assuming similar diffusion coefficients for all blend compositions, this yields a shift of the surface roughness toward lower PpMS content after

short annealing times. During this limited period of time not enough polymer could move to the surface via diffusion. As can be seen from Figure 4, the surface structures have smoothed as compared to the initial sharp structures. However, the overall rms roughness increased during annealing. Small isolated droplets which are energetically unfavorable change into larger ones (Figure 4b), and the previously flat films start to create shallow holes (Figure 4a,d). Compared to more incompatible systems such as PS:PBrS[26] or PS:PMMA,[30] the approach toward equilibrium is slow. For example, equilibrium morphologies are reached already after 12 h annealing in blend systems such as PS:PMMA[30] or after 24 h in blend systems such as PS:PBrS.[26] For PS:PMMA drastic changes such as an inversion of the morphologies after 5 min of annealing were reported.[30] In contrast to this, changes are slower in less incompatible systems. Consequently, the regular but continuous surface pattern of the PpMS:dPS = 60:40 sample has coarsened but conserved the original type of surface pattern. This is in good agreement with the lattice Boltzmann simulations of diffusive driven phase separation in binary fluids with high viscosity.[28] The corresponding master curve still exhibits a ring in Fourier space. The position of the peak maximum has shifted toward smaller inverse lengths s as observed for dPS:PB films,[32] implying that the most prominent in-plane length has increased. As Figure 8 shows, this increase is bigger for samples with smaller PpMS content. This shift in $\Lambda_{PSD}(\Phi_{PpMS})$ follows the same trend observed in $\sigma_{rms}(\Phi_{PpMS})$. Remarkably, the surface pattern of the PpMS:dPS = 80:20 sample has no peak in the master curve and thus cannot be described with one preferential in-plane length.

After 261 h Annealing. Since the overall free energy of immiscible films is lowered by minimizing the interfacial area between adjacent domains, a phase separation process will always tend to decrease the number of domains. This causes an increase of domain size. Because the examined film thickness is below the critical thickness for the built up of composition waves perpendicular to the surface, an equilibrium stage of a phase separation process will never consist of more than two or three layers. The actual number is dependent on the polymer−interface interactions.[1] After the second longer annealing step enough polymer material has been transported through the film, so that dewetting[33−38] is possible. The resulting surface structures (Figure 5) are completely different from the phase separation morphologies (Figure 3 and 4). For samples with PpMS:dPS = 60:40, 40:60, and 20:80 large drops built up. This yields an drastic increased surface roughness as pictured in Figure 6. Remarkably, the maximum of the rms roughness is further shifted toward samples with lower PpMS content Φ_{PpMS}. The drops are not arranged within the frequently observed hexagonal drop structure which is found in the case of a dry dewetting.[39] The observed drop arrangement can be regarded as a wet dewetting one.[39] Thus, the drops are in coexistence with a homogeneous film as determined with neutron reflectivity. In contrast to previous experiments on silicon substrates,[9] this layer still contains both polymers, due to the changed Hamaker constant of the float glass substrates compared to that of silicon wafers.[40] In the case of the samples with PpMS:dPS = 95:5 and 5:95 the samples have completely phase separated, and the minor component has dewetted on top of the major component. Because of the small amount of the minor component, the resulting unstable top layer is too thin to be stable and decays into droplets with a reduced diameter.[35] This explains the different size of droplets (Figure 5a,f) as compared to the micrometer drops at intermediate blend compositions(Figure 5c−e). From the analysis of the droplet volume it may be concluded that all droplets must contain some amount of the major blend component. This ensures the formation of a thin but homogeneous layer of PpMS covering all observed structures as previously measured with static SIMS.[9] Additionally, droplets of dPS on top of PpMS (Figure 5a) are larger compared to PpMS droplets on top of dPS (Figure 5f). The dewetting of PpMS on dPS was observed previously to result from a spinodal process[9] and is explainable with the Hamaker constants. A necessary condition for the presence of a spinodal dewetting process is the creation of surface morphologies which are described by one most prominent in-plane length. Because the fastest destabilizing surface wave yields the film instability, the resulting drops should have one well-defined distance. Consequently, the PSD of the corresponding SFM picture has to exhibit a ring. The droplet pattern of the sample with PpMS:dPS = 5:95 exhibits this ring which may be a sign for a spinodal process. Of course, the large drop pattern (Figure 5c−e) exhibits a peak in the master curve as well. However, this is not a proof for the presence of a spinodal process. On the other hand, the absence of any most prominent in-plane length, as observed in the case of dewetting of dPS on PpMS, is only explainable with a statistically independent process like nucleation and growth. Figure 5b,e indicates that 261 h of annealing is still not sufficiently long to reach the final equilibrium structure consisting of isolated spherical drops. Again this demonstrates that PpMS and dPS are only weakly incompatible. Additionally, it explains the large value of Λ_{PSD} for the PpMS:dPS = 20:80 sample and the missing peak in the master curve for the PpMS:dPS = 80:20 sample.

Summary

Thin polymer films are well-suited for the controlled buildup of different surface morphologies. The individual installed surface topography and internal film morphology strongly depend on the blend composition. In weakly incompatible systems, these surface structures evolve over large time scales, due to the enhanced miscibility compared to immiscible systems. This makes their control more easy. The characteristic surface morphologies of the samples right after preparation indicate that phase separation perpendicular to the surface and in-plane of the film are present during the spin-coating. The in-plane separation is constrained in quasi-two-dimensions and explainable with one most prominent in-plane length. Depending on the blend composition, flat films with smooth surfaces or dedicated small and shallow surface structures are formed. The installed enrichment layers are due to solution properties and resemble a nonequilibrium state of dPS and PpMS. Utilizing the interplay between phase separation and dewetting enables the change of these structures in depth, width, and shape. After short annealing times only the internal film structure is changed, and enrichment layers driven by surface tension and interaction are created. In contrast, the surface stays basically unchanged, despite a minor coarsening. After long

annealing times the surface topography is markedly changed as well, and large surface patterns evolve.

Summarizing all presented surface morphologies, a large range of possible applications is covered. This could have significant implications for the use of polymer blend films for the design of solid substrates.

Acknowledgment. We acknowledge the technical assistance of W. Donner and R. Günther at the EVA beamline (ILL, Grenoble) during the neutron experiments. This work was supported by the DFG Schwerpunktprogramm "Benetzung und Strukturbildung an Grenzflächen" (Sta 324/8-1), and J.S.G. acknowledges support by the GKSS project V6.1.01.G.01-HS3.

References and Notes

(1) Krausch, G. *Mater. Sci. Eng.* **1995**, *R14*, 1.
(2) Jones, R. A. L.; Norton, L. J.; Kramer, E. J.; Bates, F. S.; Wiltzius, P. *Phys. Rev. Lett.* **1991**, *66*, 1326.
(3) Bruder, F.; Brenn, R. *Phys. Rev. Lett.* **1992**, *69*, 624.
(4) Steiner, U.; Klein, J.; Fetters, L. *Phys. Rev. Lett.* **1994**, *72*, 1498.
(5) Krausch, G. *Ber. Bunsen-Ges. Phys. Chem.* **1994**, *98*, 446.
(6) Karim, A.; Slawecki, T. M.; Kumar, S. K.; Douglas, J. F.; Satija, S. K.; Han, C. C.; Russell, T. P.; Liu, Y.; Overney, R.; Sokolov, J.; Rafailovich, M. H. *Macromolecules* **1998**, *31*, 857.
(7) Jung, W. G.; Fischer, E. W. *Makromol. Chem., Macromol. Symp.* **1988**, *16*, 281.
(8) Schnell, R.; Stamm, M. *Physica B* **1997**, *234*−*236*, 247.
(9) Müller-Buschbaum, P.; O'Neill, S. A.; Affrossman, S.; Stamm, M. *Macromolecules* **1998**, *31*, 5003.
(10) Dosch, H.; Al Usta, K.; Lied, A.; Drexel, W.; Peisl, J. *Rev. Sci. Instrum.* **1992**, *63*, 5533.
(11) Lekner, J. In *Theory of Reflection*; Martinus Nijhoff Publishers: Dordrecht, 1987.
(12) Bahr, D.; Press, W.; Jebasinski, R.; Mantl, S. *Phys. Rev. B* **1993**, *47*, 4385.
(13) Stamm, M.; Schubert, D. W. *Annu. Rev. Mater. Sci.* **1995**, *25*, 325.
(14) Vignaud, G.; Gibaud, A.; Paris, F.; Ausserre, D.; Grübel, G., to be published in *Thin Solid Films*.
(15) Affrossman, S.; Henn, G.; O'Neill, S. A.; Pethrick, R. A.; Stamm, M. *Macromolecules* **1996**, *29*, 5010.
(16) Jandt, K. D.; Heier, J.; Bates, F. S.; Kramer, E. J. *Langmuir* **1996**, *12*, 3716.
(17) Kumacheva, E.; Li, L.; Winnik, M. A.; Shinozaki, D. M.; Cheng, P. C. *Langmuir* **1997**, *13*, 2483.
(18) Müller-Buschbaum, P.; Vanhoorne, P.; Scheumann, V.; Stamm, M. *Europhys. Lett.* **1997**, *40*, 655.
(19) Müller-Buschbaum, P.; Stamm, M. *Physica B* **1998**, *248*, 229.
(20) Binder, K. *Adv. Polym. Sci.* **1999**, *138*, 1.
(21) Gutmann, J. S.; Müller-Buschbaum, P.; Stamm, M. *Faraday Discuss.* **1999**, *112*, 285.
(22) Parrat, L. G. *Phys. Rev.* **1954**, *55*, 359.
(23) Born, M.; Wolf, E. In *Principles of Optics*, 2nd ed.; Pergamon Press: Oxford, 1964.
(24) James, R. W. In *The Optical Principles of the Diffraction of X-Rays*; OxBow Press: Woodbridge, CT, 1962.
(25) Müller-Buschbaum, P.; Gutmann, J. S.; Stamm, M. *J. Macromol. Sci.* **1999**, *B38*, 577.
(26) Slep, D.; Asselta, J.; Rafailovich, M. H.; Sokolov, J.; Winesett, D. A.; Smith, A. P.; Strzhemechny, Y.; Schwarz, S. A.; Sauer, B. B. *Langmuir* **1998**, *14*, 4860.
(27) Affrossman, S.; O'Neill, S. A.; Stamm, M. *Macromolecules* **1998**, *31*, 6280.
(28) Wagner, A. J.; Yeomans, J. M. *Phys. Rev. Lett.* **1999**, *80*, 1429.
(29) Schnell, R. PhD Thesis, University of Mainz, 1997.
(30) Walheim, S.; Böltau, M.; Mlynek, J.; Krausch, G.; Steiner, U. *Macromolecules* **1997**, *30*, 4995.
(31) Müller-Buschbaum, P.; Stamm, M., to be published.
(32) Sung, L.; Karim, A.; Douglas, J. F.; Han, C. C. *Phys. Rev. Lett.* **1996**, *76*, 4368.
(33) Redon, C.; Brochard-Wyart, F.; Rondelez, F. *Phys. Rev. Lett.* **1991**, *66*, 715.
(34) Redon, C.; Brzoska, J. B.; Brochard-Wyart, F. *Macromolecules* **1994**, *27*, 468.
(35) Brochard-Wyart, F.; Redon, C.; Sykes, C. *C. R. Acad. Sci., Ser. 2* **1992**, *19*, 314.
(36) Reiter, G. *Phys. Rev. Lett.* **1992**, *68*, 75.
(37) Reiter, G. *Langmuir* **1993**, *9*1344.
(38) Brochard, F.; Daillant, J. *J. Phys. (Paris)* **1990**, *68*, 1084.
(39) Fondecave, R.; Brochard-Wyart, F. *Macromolecules* **1998**, *31*, 9305.
(40) Visser, J. *Adv. Colloid Interface Sci.* **1972**, *3*, 331.

MA991073+